Two distinct surface terminations of SrVO3 (001) ultrathin films as an influential factor on metallicity

Two distinct surface terminations of $SrVO_3$ (001) ultrathin films as an influential factor on metallicity

Hirofumi Oka,[1,2,*] Yoshinori Okada,[1,3] Taro Hitosugi,[1,4] and Tomoteru Fukumura[1,2,5]

[1]WPI-Advanced Institute for Materials Research (AIMR), Tohoku University, Sendai 980-8577, Japan

[2]Core Research Cluster, Tohoku University, Sendai 980-8577, Japan.

[3]Okinawa Institute of Science and Technology Graduate University, Okinawa 904-0495, Japan

[4]Department of Chemical Science and Engineering, Tokyo Institute of Technology, Tokyo 152-8550, Japan

[5]Department of Chemistry, Tohoku University, Sendai 980-8578, Japan

∗E-mail: hirofumi.oka.e3@tohoku.ac.jp

Pulsed laser deposition-grown $SrVO_3$ (001) ultrathin films on $SrTiO_3$ (001) substrates were investigated by in situ low-temperature scanning tunneling microscopy and spectroscopy. $SrVO_3$ (001) ultrathin films showed two distinct surface terminations. One termination was a $(\sqrt{2} \times \sqrt{2})$-*R*45° reconstruction as was previously observed for $SrVO_3$ (001) thick films, while the other was a $(\sqrt{5} \times \sqrt{5})$-*R*26.6° reconstruction. Scanning tunneling spectroscopy revealed that the $(\sqrt{2} \times \sqrt{2})$-*R*45° surface shows metallic electronic structure, whereas the $(\sqrt{5} \times \sqrt{5})$-*R*26.6° surface exhibits a significantly reduced density of states at the Fermi level. These results suggest that the surface reconstruction may be an important factor to influence metallicity in epitaxial ultrathin films of transition metal oxides.

Transition metal oxides (TMO) have attracted much attention since interplay between charge, spin, and orbital degrees of freedom in correlated electrons gives rise to intriguing quantum phenomena such as high temperature superconductivity, colossal magnetoresistance, and metal-insulator transition.[1] Recent progress in oxide thin film epitaxy techniques like molecular beam epitaxy and pulse laser deposition has enabled to fabricate high quality TMO heterostructures and ultrathin films.[2,3] Engineering the heterointerfaces and ultrathin films provides a variety of functionalities being fully different from those of constituent bulk oxides, mainly due to low dimensionality and lattice strain.[4,5,6,7,8] Recently, scanning tunneling microscopy (STM) studies pointed out strong influence of surface atomic structures of substrates on the initial growth and surface atomic structure of TMO ultrathin films,[9,10] leading to unusual local electronic properties. STM combined with scanning tunneling spectroscopy (STS) is a powerful technique to investigate relation between surface atomic structures and electronic properties of TMO thin films at the atomic level.

In this paper, we report surface atomic structures and electronic properties of $SrVO_3$ (001) ultrathin films on $SrTiO_3$ (001) using in situ STM and STS at low temperatures. $SrVO_3$ (001) ultrathin films showed two distinct surface terminations exhibiting significantly different atomic and electronic structures. One termination with a ($\sqrt{5}\times\sqrt{5}$)-*R*26.6° reconstruction exhibited a significantly reduced density of states (DOS) at the Fermi level, possibly attributed to a signature of metal-insulator transition due to enhanced electron correlation at the surface of ultrathin films.[11,12] Our results highlight the importance of surface reconstruction of TMO on its electronic states, in addition to effects of well-known low dimensionality and lattice strain.

$SrVO_3$ (001) ultrathin films were epitaxially grown on Nb (0.05wt%)-doped $SrTiO_3$ (001) substrates (Shinkosha Co., Ltd.) by using pulsed laser deposition with a base pressure of 5×10^{-10} Torr. A nearly single-phase $Sr_2V_2O_7$ polycrystalline target (Kojundo Chemical Laboratory Co., Ltd.) was ablated by KrF excimer laser (λ = 248 nm) with a pulse frequency of 2 Hz and a laser fluence of 1 J/cm^2. Prior to growth, the substrates were heated at 500 °C for 30 min under ultrahigh vacuum (UHV) followed by annealing at 1000 °C for 2 hours under an oxygen partial pressure of $2 \times 10^{-7} - 2 \times 10^{-5}$ Torr. The ultrathin film was deposited at 800 °C under UHV with a deposition rate of 0.01 unit cell

(UC) per pulse, which was determined by reflection high energy electron diffraction intensity oscillations during film deposition.[13] By controlling the deposition time, the film thickness was calculated from 8 to 15 UC (approximately from 3.0 to 5.7 nm thick), being much thinner than those in a previous study.[13] After deposition, the samples at room temperature were in situ transferred to a pre-cooled STM head without breaking UHV.[14] STM and STS measurements were performed with electrochemically etched W tips at 4.7 K and 78 K, respectively. All STS measurements were performed with open feedback loop and the setpoints to stabilize a tip before opening feedback loop are indicated in figure captions.

Figure 1(a) shows a wide-range STM image of $SrVO_3$ (001) ultrathin film with atomically flat terraces separated by steps. Figure 1(b) shows a height profile along a red horizontal line in Fig. 1(a), indicating the presence of two characteristic step heights, 0.16 nm and 0.22 nm, not equal to the unit cell height of $SrVO_3$, 0.38 nm. Figure 1(c) shows a histogram of the height distribution in Fig. 1(a), in which spacing between adjacent peaks corresponds to each step height. The histogram clearly represents that the two step heights appeared alternately along the growth direction, corresponding to two kinds of surface structure as described below. Hereafter, terraces with a step height of 0.16 nm and 0.22 nm are labeled as terrace A and terrace B, respectively (see Fig. 1(a)).

Figure 2 shows high-resolution STM images (8×8 nm^2) of terraces A and B. The terrace A in Fig. 2(a) shows a square lattice of protrusions (white solid square) with a periodicity of 0.55 nm at the surface. This square lattice has been observed on $SrVO_3$ (001) thick film surfaces and identified as the ($\sqrt{2} \times \sqrt{2}$)-*R*45° reconstruction, which is formed by apical oxygen atoms on the topmost VO_2 plane concomitant with randomly distributed point defects.[13] In contrast to the previous report,[13] the density of the point defects in the ($\sqrt{2}\times\sqrt{2}$)-*R*45° reconstruction increased, and they partly arranged periodically to form another larger unit cell (white dashed diamond). Figure 2(b) reveals that the terrace B had a totally different surface structure: a square lattice of protrusions with a different periodicity of 0.84 nm (white solid square), which is larger than that of terrace A. This periodicity is approximately $\sqrt{5}$ times the lattice constant of $SrVO_3$ (001), 0.38 nm, suggesting a ($\sqrt{5}\times\sqrt{5}$)-*R*26.6° reconstruction similar to one of the most well-known surface reconstructions at $SrTiO_3$ (001).[15,16,17]

In order to clarify the azimuthal angle of the square lattice with a periodicity of 0.84 nm on the terrace B from the crystallographic direction, an STM image showing square lattices of both terraces A and B was obtained (Fig. 3(a)). Terraces A and B were separated by a step edge and square lattices were clearly observed on both the terraces. A fast Fourier transform (FFT) power spectrum map of the STM image (inset of Fig. 3(a)) shows two sets of FFT intensity maxima. The maximum closer to the origin denoted by the red arrow corresponds to the square lattice of terrace B with a longer periodicity in real space, while another maximum denoted by the blue arrow corresponds to the square lattice of terrace A. The azimuthal angle formed between the two sets of FFT intensity maxima gives the relative angle between the square lattices of terraces A and B. From an azimuthal angle of about 18° between the two maxima denoted by the arrows, the square lattice of terrace B was evaluated to rotate by about 27° from the ⟨100⟩ crystallographic directions of $SrVO_3$ (001), justifying the (√5 × √5)-*R*26.6° reconstruction of terrace B.

The coexistence of the two terminations of the (√2×√2)-*R*45° and (√5×√5)-*R*26.6° reconstructions was observed only for $SrVO_3$ (001) ultrathin films thinner than 10 UC. $SrVO_3$ (001) films with a thickness of 15 UC exhibited only the (√2×√2)-*R*45° reconstruction. The influence of $SrTiO_3$ (001) substrates on the formation of (√5×√5)-*R*26.6° reconstruction on $SrVO_3$ (001) ultrathin films is discussed in the following. The size of (√5×√5)-*R*26.6° reconstructed domains on $SrVO_3$ ultrathin films[18] increased on $SrTiO_3$ (001) substrates annealed in more reductive conditions, where larger (√5×√5)-*R*26.6° reconstructed domains are expected to be formed on.[17,19] This result indicates a strong correlation between the formation of (√5×√5)-*R*26.6° reconstruction on $SrVO_3$ (001) ultrathin films and that on $SrTiO_3$ (001) substrates. The important point here is that the (√5×√5)-*R*26.6° reconstruction of $SrTiO_3$ (001) is caused by the large amount of oxygen deficiencies in the bulk and nonstoichiometry of Sr and Ti atoms near the surface.[19] At the initial stage of growing $SrVO_3$ on $SrTiO_3$ (001) substrate, nonstoichiometry near the surface of $SrTiO_3$ should affect the growth and nonstoichiometry of $SrVO_3$ ultrathin films. It is reasonable to consider that this effect results in the formation of the (√5×√5)-*R*26.6° reconstruction on $SrVO_3$ ultrathin film surfaces. As the thickness of $SrVO_3$ increases, the effect of the $SrTiO_3$ substrate decreases and the ratio of Sr and V atoms is governed by the target composition and pulsed laser

deposition processes. Accordingly, we speculate that the (√5×√5)-*R*26.6° reconstruction was not formed on $SrVO_3$ ultrathin films.

To reveal the atomic structure model of the (√5×√5)-*R*26.6° reconstruction, bias-dependent STM measurements were performed. Although the square lattice of the (√2×√2)-*R*45° reconstruction showed negligible bias dependent images within the bias voltages of ±2 V, the (√5×√5)-*R*26.6° reconstruction showed strong bias dependence. To explain this bias dependence, a positive-bias-voltage STM image was overlaid on a negative-bias voltage image at the corresponding site in Fig. 3(b). In addition to protrusions forming the (√5×√5)-*R*26.6° square lattice observed at positive bias voltages (an inset of Fig. 3(b)), smaller protrusions in between them were observed at negative bias voltages around −1.0 V (Fig. 3(b)). An atomically resolved STM image at a bias voltage of −1.0 V in Fig. 3(b) resolved (1) a protrusion (light blue circle) at the edge of the white square and (2) a four-clustered protrusion (light blue square) with the edge of 0.26 nm at the center of the white square. The edge length is similar to that between oxygen atoms in the VO_2 plane of $SrVO_3$ (001), 0.27 nm. These two features are the same as those observed for a 'Sr adatom model' of the (√5×√5)-*R*26.6° reconstruction on the topmost TiO_2 plane of $SrTiO_3$ (001).[16,17,20] Atomic structure models of the (√2×√2)-*R*45° and (√5×√5)-*R*26.6° reconstructions are given in Fig. 3(c).

We here point out the unresolved issue of the surface atomic structures. Previous studies on the (√2×√2)-*R*45° reconstruction of $SrVO_3$ and $LaMnO_3$ reported that the reconstructions is formed by apical oxygen atoms on the topmost MO_2 plane of perovskite RMO_3 (001), where *R* and *M* are alkaline earth and transition metal cations, respectively.[13, 21] Thus, the (√2×√2)-*R*45° reconstruction observed in this study corresponds to oxygen atoms of a SrO plane on topmost VO_2 plane of $SrVO_3$ (001) (Fig. 3(c)). However, this result is inconsistent with the fact that the (√5×√5)-*R*26.6° reconstruction also corresponds to a SrO plane according to the Sr adatom model, because the (√2×√2)-*R*45° and (√5×√5)-*R*26.6° reconstructions were observed on different planes of $SrVO_3$ (001) separated by 0.16 or 0.22 nm in height. Further experimental and theoretical studies especially on the initial growth of $SrVO_3$ are required to resolve this contradiction.

In order to investigate local electronic structure, differential conductance (dI/dV) spectra on the terraces of (√2×√2)-R45° and (√5×√5)-R26.6° reconstructions are shown in Fig. 4. Each spectrum was obtained by averaging over more than fifty spectra measured on clean and flat terraces. The measured dI/dV signal is proportional to the local DOS of the sample.[22] The dI/dV spectrum of the (√2×√2)-R45° reconstruction shows a broad peak at +0.4 V and minima at −0.55 and +0.8 V, being consistent with a metallic DOS in a previous study for 20 nm thick $SrVO_3$ (001) films.[13] In contrast, the dI/dV spectrum of the (√5×√5)-R26.6° reconstruction shows strongly reduced DOS around the Fermi level (*i.e*. zero bias voltage) and a maximum at +0.5 V. The standard deviation is found to be larger for the spectrum of the (√5×√5)-R26.6° reconstruction. This can be ascribed to the position dependence of dI/dV signal within the unit cell of the (√5×√5)-R26.6° reconstruction. Our position-dependent dI/dV spectra on the (√5×√5)-R26.6° reconstruction (not shown) revealed that the overall shape of the spectra was very similar to each other, but the intensity slightly changed within the unit cell, which is consistent with the above result that high resolution STM images showed bias dependence on the (√5×√5)-R26.6° reconstruction (Fig. 3(b)). However, the reduced DOS around the Fermi level did not depend on the position within the unit cell of the (√5×√5)-R26.6° reconstruction. Thus, the dI/dV spectra in Fig. 4 imply the strong influence of the surface reconstruction on the local electronic structure of $SrVO_3$ (001) ultrathin films.

In the following, the possibility that the surface reconstruction influences the local electronic structure of $SrVO_3$ (001) ultrathin films is discussed. Yoshimatsu *et al*. found metal-insulator transition in $SrVO_3$ (001) ultrathin films using photoemission spectroscopy and attributed it to band narrowing caused by the decreased film thickness.[12] First-principles calculations predicted that the electron correlation is enhanced at the VO_2-terminated $SrVO_3$ (001) surface due to band narrowing and orbital-dependent charge transfer,[11] probably leading to the metal-insulator transition at the VO_2-terminated $SrVO_3$ (001) surface. Indeed, the terrace with the (√5×√5)-R26.6° reconstruction of $SrVO_3$ (001) ultrathin films was composed of VO_2-terminated surface with Sr adatoms (Sr adatom model) and the VO_2-terminated surface was observed in the atomically resolved STM image (Fig. 3(b)). On the other hand, the terrace with the (√2×√2)-R45° reconstruction was covered with apical oxygen atoms and the VO_2-terminated surface was not visible

with STM since the adsorption of apical oxygen atoms induces two-dimensional surface states.[13] Thus, both the band narrowing effect and the enhanced electron correlation are expected at the (√5×√5)-*R*26.6° surface (terrace B). Since the (√5×√5)-*R*26.6° surface is only observed in ultrathin films, these results suggest that the surface reconstruction may influence the metallicity in $SrVO_3$ (001) ultrathin films.

In conclusion, in situ STM and STS measurements clearly revealed that $SrVO_3$ (001) ultrathin films on $SrTiO_3$ (001) have two distinct surface terminations with different surface atomic and electronic structures: the (√2×√2)-*R*45° reconstruction with metallic DOS and the (√5×√5)-*R*26.6° reconstruction with strongly reduced DOS around the Fermi level. The latter was observed only for ultrathin films. These results indicate that the surface reconstruction may be a hidden factor to determine the local electronic states of ultrathin TMO, providing a route to engineer electronic properties of TMO films. In addition, the control of surface reconstructions should affect the initial growth processes of thin films, and eventually influence the electronic properties of films and heterointerfaces.

Acknowledgment

The study was supported by JSPS KAKENHI (17H02779, 18H03876, 26105002, 18K18935).

Figure 1: (a) Wide-range STM image of $SrVO_3$ (001) ultrathin films with a thickness of 10 UC (sample bias voltage (V) = 0.3 V, tunneling current (I) = 6 pA, 450 × 450 nm^2, and temperature (T) = 4.7 K). Each terrace is labeled as A or B depending on the step height. (b) Height profile along the red horizontal line in (a). The lowest terrace height was set to zero. (c) Histogram of the height distribution of the STM image in (a).

Figure 2: High-resolution STM images of (a) terrace A and (b) terrace B of $SrVO_3$ (001) ultrathin films with a thickness of 10 UC. Unit cells of the structures are indicated by the white squares. The dashed diamond in (a) shows another unit cell due to the periodically arranged defects. (a) V = 0.3 V, I = 6 pA, 8 × 8 nm^2, and 4.7 K. (b) V = 1.0 V, I = 50 pA, 8 × 8 nm^2, and T = 4.7 K.

Figure 3: (a) High-resolution STM image around a step between terraces A and B of $SrVO_3$ (001) ultrathin film with a thickness of 10 UC. V = 1.0 V, I = 50 pA, 18 × 18 nm^2, and T = 4.7 K. Inset: fast Fourier transform (FFT) map of the STM image in (a). The arrows in blue and red indicate FFT intensity maxima. The bright cross is caused by the step structure. (b) Atomically resolved STM image of the (√5×√5)-*R*26.6° structure (terrace B). V = −1.0 V, I = 40 pA, 5 × 10 nm^2, and T = 4.7 K. Inset: STM image of the (√5×√5)-*R*26.6° structure obtained at a positive bias voltage. V = +1.5 V, I = 60 pA, 2 × 3.5 nm^2, and T = 4.7 K. The white squares show a unit cell of the (√5×√5)-*R*26.6° structure and an equivalent site for positive- and negative-bias voltage STM images. In addition to the protrusions visible in the inset at V = +1.5 V, protrusions (light blue circles) and four-clustered protrusions (light blue square) appeared at V = −1.0 V. (c) Schematics of top and side views of the (√2×√2)-*R*45° and (√5×√5)-*R*26.6°reconstructions.

Figure 4: Differential conductance (d*I*/d*V*) spectra on a terrace A [(√2×√2)-*R*45° reconstruction] and a terrace B [(√5×√5)-*R*26.6° reconstruction] of $SrVO_3$ (001) ultrathin film with a thickness of 8 UC. Each spectrum was obtained by averaging over more than fifty spectra. The standard deviation gives error bars shaded in light colors. $V = -1.3$ V, $I = 10$ pA, and $T = 78$ K.

References

[1] Y. Tokura and N. Nagaosa, Science **288**, 462468 (2000).

[2] D. Oka and T. Fukumura, CrystEngComm **19**, 21442162 (2017).

[3] M. Brahlek, A. S. Gupta, J. Lapano, J. Roth, H.-T. Zhang, L. Zhang, R. Haislmaier, and R. Engel-Herbert, Adv. Funct. Mater. **28**, 1702772 (2018).

[4] A. Ohtomo and H. Y. Hwang, Nature **427**, 423426 (2004).

[5] A. Brinkman, M. Huijben, M. van Zalk, J. Huijben, U. Zeitler, J. C. Maan, W. G. van der Wiel, G. Rijnders, D. H. A. Blank, and H. Hilgenkamp, Nat. Mater. **6**, 493496 (2007).

[6] N. Reyren, S. Thiel, A. D. Caviglia, L. F. Kourkoutis, G. Hammerl, C. Richter, C. W. Schneider, T. Kopp, A.-S. Rüetschi, D. Jaccard, M. Gabay, D. A. Muller, J.-M. Triscone, and J. Mannhart, Science **317**, 11961199 (2007).

[7] K. Yoshimatsu, K. Horiba, H. Kumigashira, T. Yoshida, A. Fujimori, M. Oshima, Science **333**, 319322 (2011).

[8] J. Matsuno, N. Ogawa, K. Yasuda, F. Kagawa, W. Koshibae, N. Nagaosa, Y. Tokura, and M. Kawasaki, Sci. Adv. **2**, e1600304 (2016).

[9] Y. J. Chang and S.-H. Phark, Curr. Appl Phys. **17**, 640656 (2017).

[10] K. Iwaya, T. Ohsawa, R. Shimizu, Y. Okada, and T. Hitosugi, Sci. Technol. Adv. Mater. **19**, 282290 (2018).

[11] H. Ishida, D. Wortmann, and A. Liebsch, Phys. Rev. B **73**, 245421 (2006).

[12] K. Yoshimatsu, T. Okabe, H. Kumigashira, S. Okamoto, S. Aizaki, A. Fujimori, and M. Oshima, Phys. Rev. Lett. **104**, 147601 (2010).

[13] Y. Okada, S.-Y. Shiau, T.-R. Chang, G. Chang, M. Kobayashi, R. Shimizu, H.-T. Jeng, S. Shiraki, H. Kumigashira, A. Bansil, H. Lin, and T. Hitosugi, Phys. Rev. Lett. **119**, 086801 (2017).

[14] K. Iwaya, R. Shimizu, T. Hashizume, and T. Hitosugi, Rev. Sci. Instrum. **82**, 083702 (2011).

[15] H. Tanaka, T. Matsumoto, T. Kawai, and S. Kawai, Jpn. J. Appl. Phys. **32**, 1405 (1993).

[16] T. Kubo and H. Nozoye, Phys. Rev. Lett. **86**, 18011804 (2001).

[17] D. T. Newell, A. Harrison, F. Silly, and M. R. Castell, Phys. Rev. B **75**, 205429 (2007).

[18] A domain boundary can be seen in the upper part of Fig. 2(b).

[19] R. Shimizu, K. Iwaya, T. Ohsawa, S. Shiraki, T. Hasegawa, T. Hashizume, and T. Hitosugi, Appl. Phys. Lett. **100**, 263106 (2012).

[20] I. Shiraki and K. Miki, Surf. Sci. **605**, 13041307 (2011).

[21] K. Fuchigami, Z. Gai, T. Z. Ward, L. F. Yin, P. C. Snijders, E. W. Plummer, and J. Shen, Phys. Rev. Lett. **102**, 066104 (2009).

[22] H. Oka, O. O. Brovko, M. Corbetta, V. S. Stepanyuk, D. Sander, and J. Kirschner, Rev. Mod. Phys. **86**, 1127 (2014), and references therein.

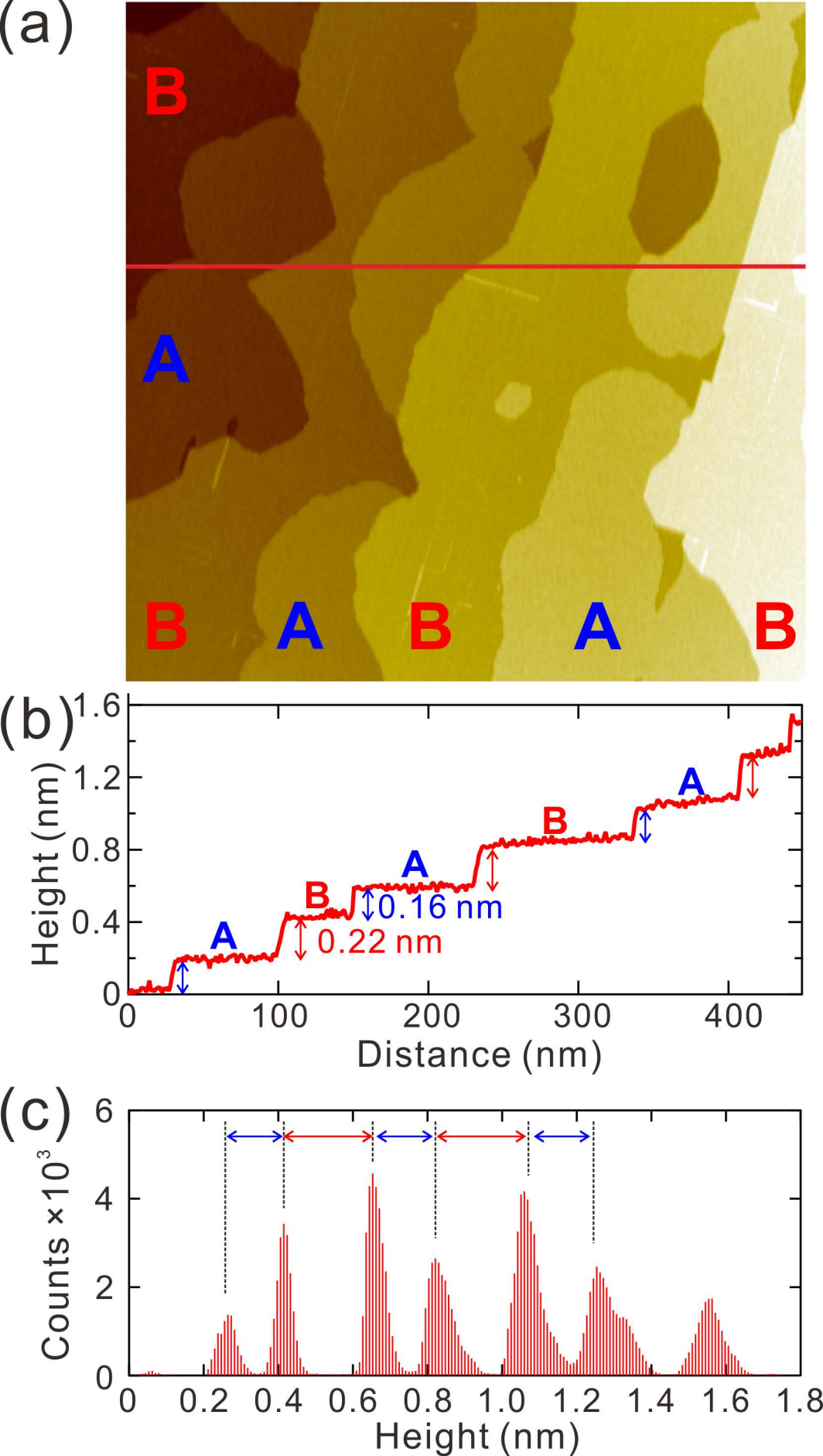
(a)
B
A
B A B A B
(b)
Height (nm)
Distance (nm)
A
B
A
B
A
0.16 nm
0.22 nm
(c)
Counts ×10^3
Height (nm)

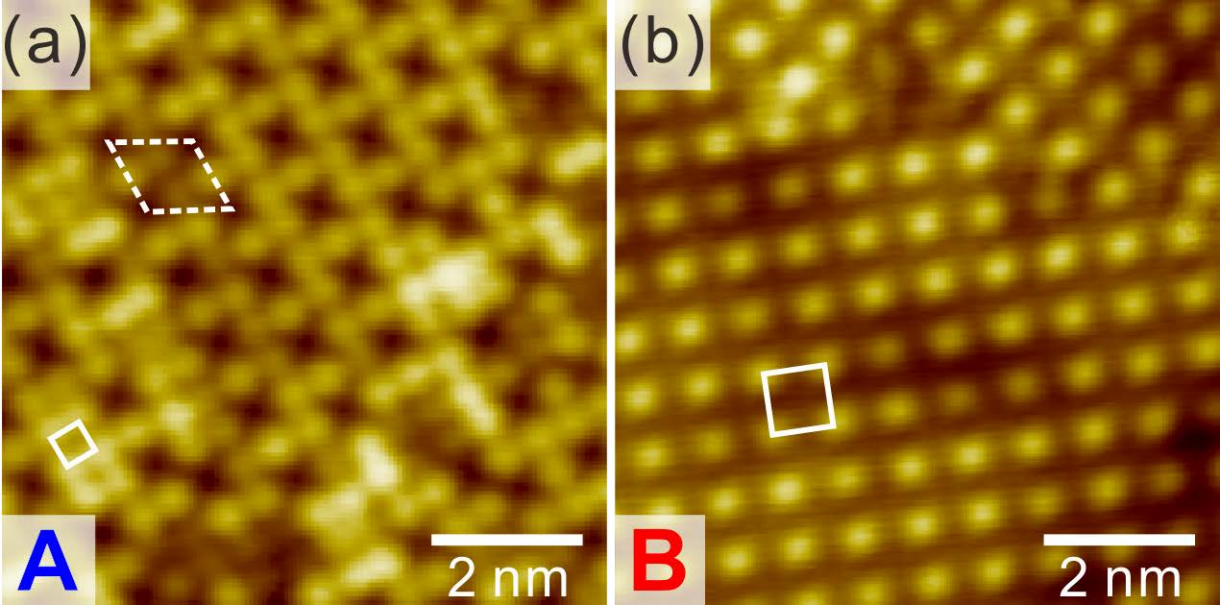
(a)
A
2 nm
(b)
B
2 nm

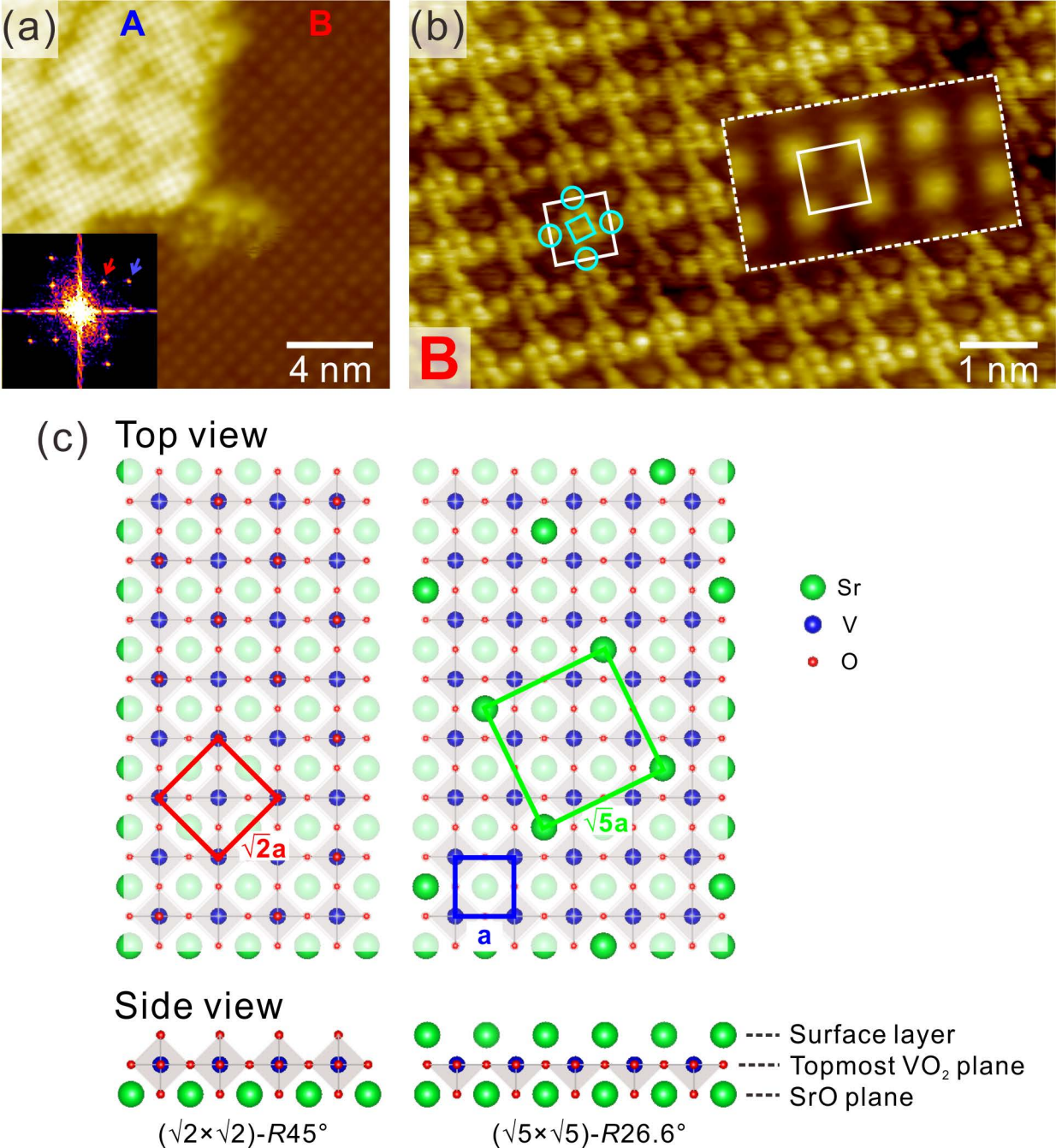
(a)
A
B
4 nm
(b)
B
1 nm
(c)
Top view
√2a
√5a
a
Sr
V
O
Side view
Surface layer
Topmost VO2 plane
SrO plane
(√2×√2)-R45°
(√5×√5)-R26.6°

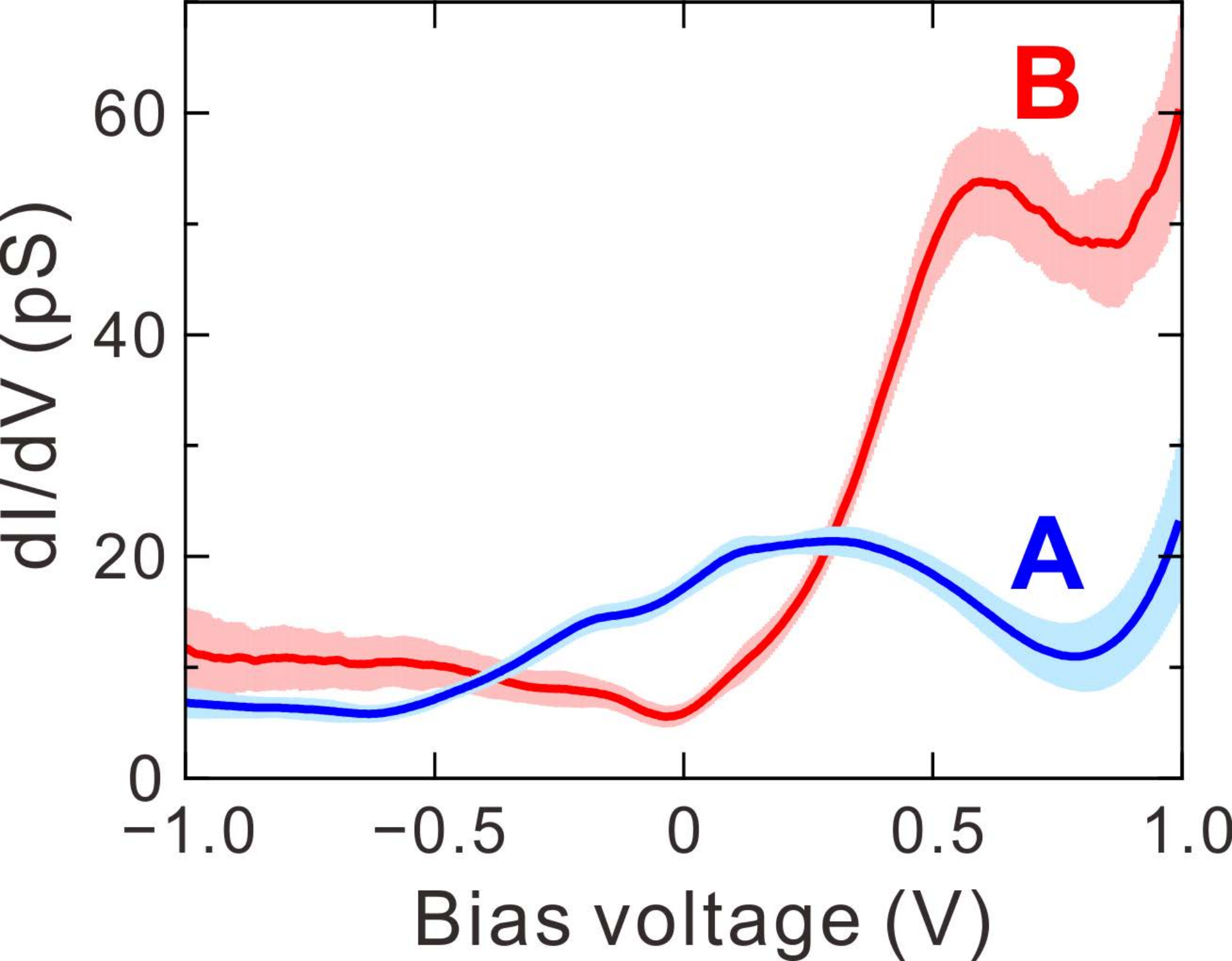
B
A
60
40
20
0
dI/dV (pS)
−1.0
−0.5
0
0.5
1.0
Bias voltage (V)